

On Neutrosophic Extension of the Maxwell Model: Properties and Applications

Zahid Hossain Khan


Journal of Function Spaces

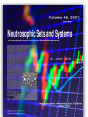
Cite this paper

Downloaded from [Academia.edu](#) 

[Get the citation in MLA, APA, or Chicago styles](#)

Related papers

[Download a PDF Pack](#) of the best related papers 



[Neutrosophic Sets and systems, Vol. 46, 2021](#)

Florentin Smarandache

[Neutrosophic Sets and Systems, Vol. 46, 2021](#)

Florentin Smarandache

[Neutrosophic Sets and Systems, Vol. 45, 2021](#)

Florentin Smarandache

Research Article

On Neutrosophic Extension of the Maxwell Model: Properties and Applications

Faisal Shah,¹ Muhammad Aslam,¹ Zahid Khan ,² Mohammed M. A. Almazah ,^{3,4} and Fuad S. Alduais^{5,6}

¹Department of Mathematics and Statistics, Riphah International University, Islamabad 45210, Pakistan

²Department of Mathematics and Statistics, Hazara University Mansehra, Dhodial, Pakistan

³Department of Mathematics, College of Sciences and Arts (Muhiyl), King Khalid University, Muhiyl 61421, Abha, Saudi Arabia

⁴Department of Mathematics and Computer, College of Sciences, Ibb University, Ibb 70270, Yemen

⁵Department of Mathematics, College of Science and Humanities in Al-Kharj, Prince Sattam Bin Abdulaziz University, 11942 Al-Kharj, Saudi Arabia

⁶Country Business Administration Department, Administrative Science College, Tamar University, Tamar, Yemen

Correspondence should be addressed to Zahid Khan; zahidkhan@hu.edu.pk

Received 16 December 2021; Accepted 19 January 2022; Published 16 February 2022

Academic Editor: Muhammad Gulzar

Copyright © 2022 Faisal Shah et al. This is an open access article distributed under the Creative Commons Attribution License, which permits unrestricted use, distribution, and reproduction in any medium, provided the original work is properly cited.

This work presents the neutrosophic Maxwell distribution (NMD) as a novel probability distribution. The proposed model represents a generalized design of Maxwell distribution that provides more analytical flexibility for data, including all imprecise observations or some degree of vagueness within the dataset. Important reliability characteristics and distributional properties of NMD are developed under the notion of neutrosophy. The neutrosophic forms of some commonly used functions in applied statistics such as mean, variance, moment generating function, and shape coefficients are explored. In view of uncertainties involved in the processing data and indeterminacy in the defined parameters, an estimation framework using the maximum likelihood approach is established. Additionally, the quantile function is developed to validate the distributional properties of NMD. The efficiency of the neutrosophic estimate has been studied through a Monte Carlo simulation. Finally, real data on the incubation period of COVID-19 are considered for numerical illustration, and further extensions of the NMD for future research works are discussed.

1. Introduction

Maxwell [1] derived a mathematical formulation of Maxwell distribution to illustrate the distribution of particles in thermal equilibrium. The unimodal and leptokurtic structure of the Maxwell curve is yielded due to the fact that all molecules do not travel with identical velocity, and some move faster than others [2]. A lot of fundamental characteristics of gases are explained by the Maxwell model, which impacts kinetic energy [3]. The Maxwell distribution is also known as the model of momenta, velocity, the degree of momenta, and energy of particles [4]. The Maxwell distribution is well-known for its applications in astronomy,

chemistry, and engineering [5]. The failure rate of the Maxwell distribution rises steadily over time, which makes it effective in reliability and in life-testing experiments when the assumption of fixed failure rates, like that of an exponential distribution, is impractical [6]. Among many notable contributions that recommended this distribution in real-world testing investigations are [7–10]. For the first time, the Maxwell model was treated as a lifetime distribution and described the Bayesian estimators for the reliability function and the parameter in the study [11]. Chaturvedi and Rani [12] extended the Maxwell model by adding more parameters and provided Bayesian and classical estimators. The empirical Bayesian estimator using the Maxwell model is investigated

by [13]. In these works, authors considered that known information about studied variables and distributional parameters are completely specified. The earlier studies devoted a mathematical treatment to the Maxwell model but do not throw light on neutrosophic aspects of the Maxwell probability function, especially in applied statistical research.

We encounter continuous variables in everyday life, and the observations are defined in exact numbers. There are hundreds of continuous univariate distributions found in the applied statistical applications [14]. Over the last several decades, various distributions have been extensively utilized to model data in a wide range of areas such as environmental sciences, actuarial and engineering, medical sciences, biological research, insurance, and economics. However, the common distributions do not suit well to every data in various circumstances [15]. On the other hand, measurements of any continuous variables always have some degree of imprecision [16]. It is self-evident in the scientific realm of measurements that terms like “equality” and “exact” should be forbidden since continuous processes cannot be measured precisely [17]. In addition to continuous variables, there are circumstances when accurate measurements are not feasible due to the irregular nature of studied variables [18–21]. As an illustration, it is impossible to estimate a river’s depth precisely due to the wave nature of water. A similar problem arises when attempting to differentiate between a healthy and an unhealthy individual, a bad and good student, or between a normal and cool body temperature. This results in the single measurement being distorted. These considerations lead to the conclusion that real measurements do contain errors or imprecision in individual observations, which is referred to as fuzziness [22]. In a classical statistical framework, modeling variability among data is usually performed without accounting for fuzziness. Smarandache [23] proposed neutrosophic logic, which is an extension of fuzzy logic in order to tackle the uncertainties in studied variables. Smarandache [24] also provided the notions of neutrosophic statistics, which are generalizations of classical statistical procedures. When indeterminacy is zero, the neutrosophic statistical method converges to the classical approach. Valuable works that promoted the idea of neutrosophic statistics and undetermined statistics can be found in [25–27]. Sherwani et al. [28] recently developed neutrosophic statistics in applied distributional theory. Based on a review of the literature and to the best of our knowledge, there is no study on the neutrosophic design of the Maxwell model for dealing with data that may be imprecisely defined.

In what follows, this study presents a statistical framework of the neutrosophic Maxwell distribution with applications, particularly in applied statistical research. Neutrosophic measures under the Maxwell model have been developed for handling imprecise data.

The work done in this study is divided into sections as follows. In Section 2, the proposed NMD, its genesis, some distributional properties, related theorems, and reliability characteristics are given. Section 3 deals with the maximum likelihood estimation under the neutrosophic environment. An extensive simulation work to validate the model

authenticity is conducted in Section 4. In Section 5, the applicability of NMD has been illustrated by analyzing a real dataset on COVID-19 incubation period. Last, in Section 6, a brief discussion about the work done has been concluded.

2. Neutrosophic Maxwell Distribution

The neutrosophic random variable W is followed by the NMD model with probability density function ($P DF_N$) as

$$\phi_N(w) = \sqrt{\frac{2}{\pi}} \lambda_N^{-3} w^2 e^{-(w^2/2\lambda_N^2)} \frac{w^2}{2\lambda_u^2} I_{(0,\infty)}(w); \quad w > 0, \quad (1)$$

where $\lambda_N \in [\lambda_l, \lambda_u]$, I is an indicator function, W is a nonnegative variable, and subscripts l and u , respectively, indicate the lower value and upper value of an indeterminate parameter. The neutrosophic density function ($P DF_N$) indicates the chance of events happening between two values under the sturdy curve. In the framework of neutrosophic calculus, it is defined as the integral of the variable density over a specified range. The neutrosophic parameter λ_N denotes simply the scale factor whose different values result in a variety of neutrosophic curves of the proposed distribution. The graph of $P DF_N$ for a continuous random variable W with different neutrosophic parameters is shown in Figure 1.

Figure 1 shows that the densities are asymmetric and skewed toward the right. In the neutrosophic framework, the density curve is represented by a thick layer rather than a single curve. The layer thickness (shaded region) corresponds to an indeterminacy part and total area under the sturdy curve equal to one due to completeness of $P DF_N$. Several other supporting properties of NMD may be constructed in the following versions of the theorems.

Theorem 1. *The distribution function of NMD is $(2/\sqrt{\pi})\gamma[(3/2), (w^2/2\lambda_N^2)]$.*

Proof. Distribution function is conventionally defined as

$$\begin{aligned} \eta_N(w) &= P_N(W \leq w) \\ &= \int_0^w [\phi_l(w), \phi_u(w)] dw \\ &= \left[\int_0^w \phi_l(w) dw, \int_0^w \phi_u(w) dw \right]. \end{aligned} \quad (2)$$

Using the transformation $x = (w^2/2\lambda_l^2)$ and $y = (w^2/2\lambda_u^2)$ in equation (2) yielded

$$\begin{aligned} \eta_N(w) &= \left[\frac{2}{\sqrt{\pi}} \int_0^{(w^2/2\lambda_l^2)} y^{(1/2)} e^{-y} dy, \right. \\ &\quad \left. \frac{2}{\sqrt{\pi}} \int_0^{(w^2/2\lambda_u^2)} x^{(1/2)} e^{-x} dx \right]. \end{aligned} \quad (3)$$

Further simplification of equation (3) resulted

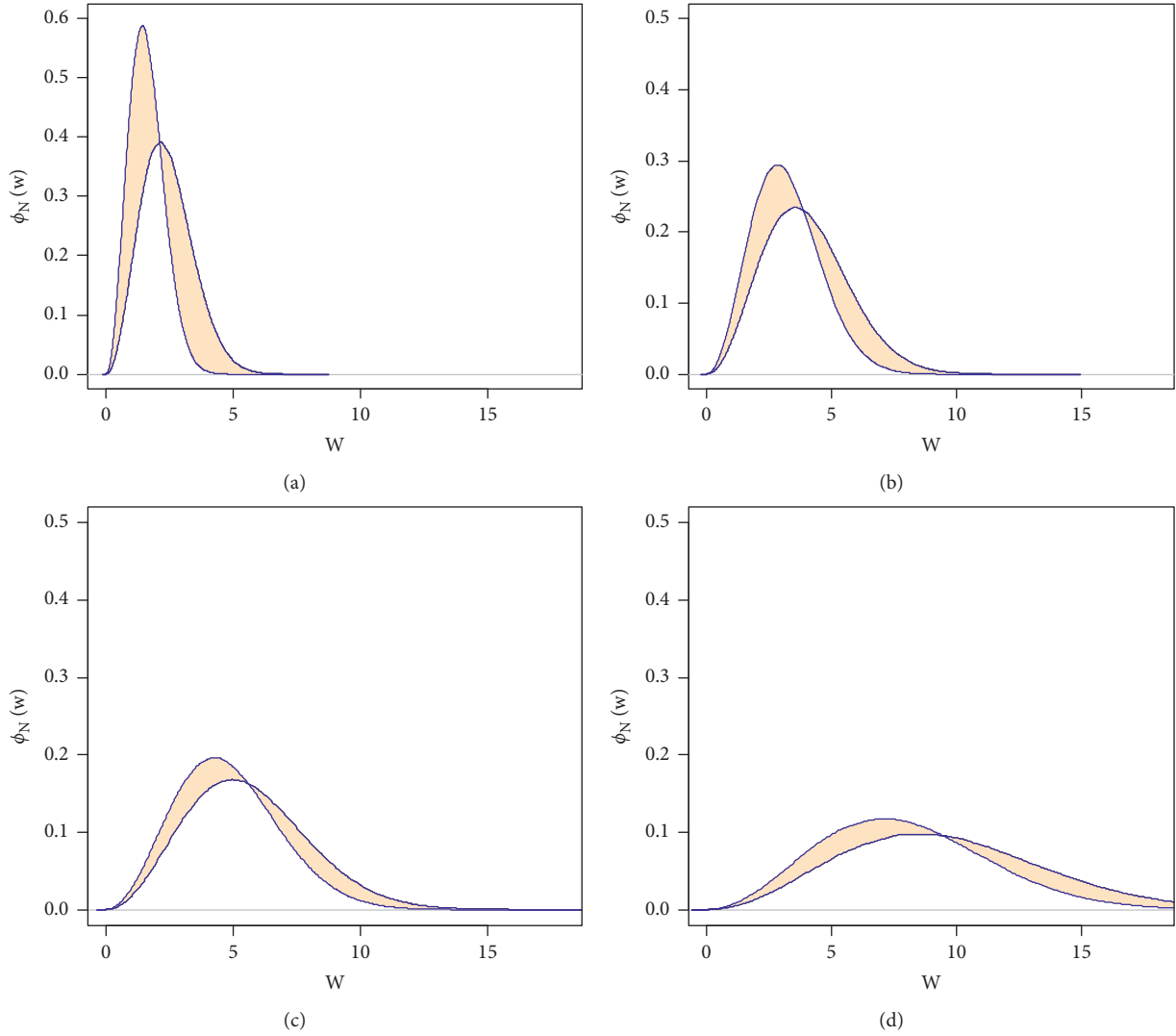


FIGURE 1: Density plots of the NMD at different values of the neutrosophic parameter. (a) $\lambda_N = (1, 1.5)$. (b) $\lambda_N = (2, 2.5)$. (c) $\lambda_N = (3, 3.5)$, (d) $\lambda_N = (5, 6)$.

$$\eta_N(w) = \left[\frac{2\gamma((3/2), (w^2/2\lambda_u^2))}{\sqrt{\Pi}}, \frac{2\gamma((3/2), (w^2/2\lambda_l^2))}{\sqrt{\Pi}} \right] \quad (4)$$

$$= \frac{2}{\sqrt{\pi}} \gamma \left[\frac{3}{2}, \frac{w^2}{2\lambda_N^2} \right],$$

where $\gamma(\cdot)$ is the incomplete gamma function. The function $\eta_N(w)$ has the counter domain $(0, 1)$, and the domain is a real line with nondecreasing and monotone behavior. Like $P DF_N$, it is also represented by a thick curve, as shown in Figure 2.

Figure 2 shows the overall behavior of $\eta_N(w)$ which is right continuous and varies in the interval $(0, 1)$. \square

Theorem 2. *The neutrosophic mean of the NMD is $2\lambda_N\sqrt{2/\pi}$.*

Proof.

$$\begin{aligned} E(W) &= \int_0^\infty w \phi_N(w) dw \\ &= \int_0^\infty w [\phi_l(w), \phi_u(w)] dw \\ &= \left[\int_0^\infty w \phi_l(w) dw, \int_0^\infty w \phi_u(w) dw \right] \quad (5) \\ &= \left[2\lambda_l \sqrt{\frac{2}{\pi}}, 2\lambda_u \sqrt{\frac{2}{\pi}} \right] \\ &= 2\lambda_N \sqrt{\frac{2}{\pi}}, \end{aligned}$$

is the required result. \square

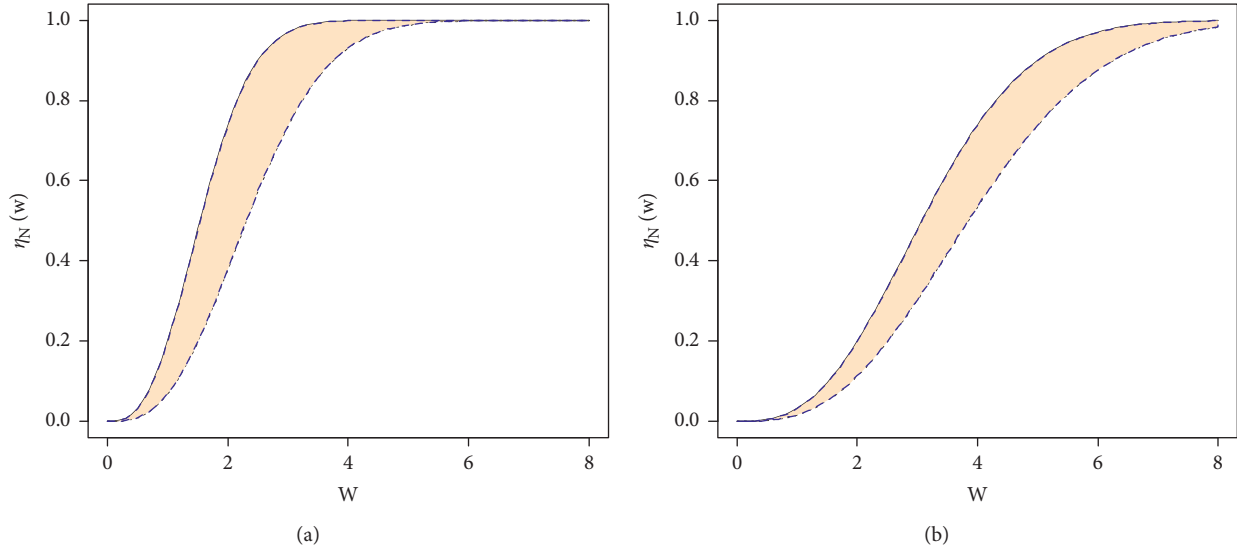


FIGURE 2: Neutrosophic distribution function curves of the Maxwell model with different values of λ_N . (a) $\lambda_N = (1, 1.5)$. (b) $\lambda_N = (2, 2.5)$.

Theorem 3. The variance of NMD is $(3\pi - 8)(\lambda_N^2/\pi)$.

Proof. Definition of variance is

$$\sigma_N^2(w) = E(W^2) - (E(W))^2, \quad (6)$$

where

$$E(W) = 2\lambda_N \sqrt{\frac{2}{\pi}}, \quad (7)$$

and

$$\begin{aligned} E(W^2) &= \int_0^\infty w^2 \phi_N(w) dw \\ &= \int_0^\infty w^2 [\phi_l(w), \phi_u(w)] dw \\ &= \left[\int_0^\infty w^2 \phi_l(w) dw, \int_0^\infty w^2 \phi_u(w) dw \right] \\ &= [3\lambda_l^2, 3\lambda_u^2] \end{aligned} \quad (8)$$

$$E(W^2) = 3\lambda_N^2.$$

Thus, equation (6) becomes.

Now, $\sigma_N^2(w) = [3\lambda_l^2, 3\lambda_u^2] - ([2\lambda_l \sqrt{2/\pi}, 2\lambda_u \sqrt{2/\pi}])^2$.

After simplifying, we get

$$\begin{aligned} &= (3\pi - 8) \frac{\lambda_l^2}{\pi}, (3\pi - 8) \frac{\lambda_u^2}{\pi} \\ &= (3\pi - 8) \frac{\lambda_N^2}{\pi}. \end{aligned} \quad (9)$$

□

Theorem 4. The r^{th} moment about the origin of NMD is $(2^{(r+2/2)}/\sqrt{\pi})\lambda_N^r \Gamma(r+3/2)$.

Proof. The r^{th} moment by definition is given by

$$\begin{aligned} \mu_r' &= E(W)^r = \int_0^\infty w^r \phi_N(w) dw \\ &= \int_0^\infty w^r [\phi_l(w), \phi_u(w)] dw \\ &= \left[\int_0^\infty w^r \phi_l(w) dw, \int_0^\infty w^r \phi_u(w) dw \right] \\ &= \left[\frac{2^{(r+2/2)}}{\sqrt{\pi}} \lambda_l^r \Gamma\left(\frac{r+3}{2}\right), \frac{2^{(r+2/2)}}{\sqrt{\pi}} \lambda_u^r \Gamma\left(\frac{r+3}{2}\right) \right] \\ \mu_r' &= \frac{2^{(r+2/2)}}{\sqrt{\pi}} \lambda_N^r \Gamma\left(\frac{r+3}{2}\right). \end{aligned} \quad (10)$$

□

Theorem 5. The skewness of the NMD is $(2\sqrt{2}(16-5\pi)/(3\pi-8)^{(3/2)})$.

The skewness coefficient is defined by $\sqrt{\beta_1}$, where

$$\beta_1 = \frac{\mu_3'}{\mu_2'^3}, \quad (11)$$

and

$$\begin{aligned} \mu_2 &= \mu_2' - (\mu_1')^2 \\ \mu_3 &= \mu_3' - 3\mu_2'\mu_1' + 2(\mu_1')^3. \end{aligned} \quad (12)$$

So, equation (11) becomes

$$\sqrt{\beta_1} = \sqrt{\frac{[(16-5\pi)(2\sqrt{2}/\pi)^{(3/2)}\lambda_N^3]^2}{[(3\pi-8)(\lambda_N^2/\pi)]^3}}. \quad (13)$$

Thus, further simplification of equation (13) yielded

$$\sqrt{\beta_1} = \frac{2\sqrt{2}(16 - 5\pi)}{(3\pi - 8)^{(3/2)}}. \quad (14)$$

Theorem 6. The kurtosis of NMD is given by $(4(-96 + 40\pi - 3\pi^2)/(3\pi - 8)^2)$.

Proof. Definition kurtosis coefficient is given by

$$= \beta_2 - 3, \quad (15)$$

where

$$\beta_2 = \frac{\mu_4}{\mu_2^2}, \quad (16)$$

and

$$\mu_4 = \mu_4' - 4\mu_1'\mu_3' + 6(\mu_1')^2\mu_2' - 3(\mu_1')^4. \quad (17)$$

Thus, using equations (9) and (17) in equation (16) yielded

$$\text{Kurtosis - coefficient} = \frac{(15\pi^2 + 16\pi - 192)(\lambda_N^4/\pi^2)}{[(3\pi - 8)(\lambda_N^2/\pi)]^2} - 3, \quad (18)$$

or

$$\text{Kurtosis - coefficient} = \frac{4(-96 + 40\pi - 3\pi^2)}{(3\pi - 8)^2}. \quad (19)$$

In this section, we also considered several to illustrate the theoretical results of the proposed model. \square

Example 1. If the time taken by the service station employee for wheels alignment is a random variable that follows NMD with parameter $\lambda_N = [5, 8]$, determine the probability that the attendant would take more than 15 minutes to balance four tires.

Solution: . Let W be a random variable that represents the number of times (in minutes) that a service station employee takes to balance tires; then, the required probability would be

$$P(w > 15) = 1 - P(W \leq 15). \quad (20)$$

Using equation (2), we can write

$$P(w > 15) = 1 - \eta_N(15). \quad (21)$$

By using $\lambda_N = [5, 8]$, equation (20) can be further simplified as

$$P(w > 15) = 1 - [0.681, 0.971] = [0.029, 0.319]. \quad (22)$$

Example 2. Research published in the November 1990 edition of Chemical Engineering Progress (CEP) magazine addressed the percentage purity of neon gas from a specific supplier. Assume that the percentage purity distribution was

NMD with a mean of [92, 95] percent. What proportion of the purity values is expected to be between 97 and 99?

Solution: . Let W be a random variable that denotes the percentage purity of neon gas.

Now, $E(W) = [92, 95]$.

Using the result given in Theorem 2, we can find

$$\lambda_N = [115, 119]. \quad (23)$$

Using Theorem 1, we can write

$$P(97 \leq w \leq 99) = \eta_N(99) - \eta_N(97) \\ = [0.125, 0.137] - [0.118, 0.129]. \quad (24)$$

Hence,

$$P(97 \leq w \leq 99) = [0.007, 0.008] \approx [0.07, 0.08]\%. \quad (25)$$

Example 3. Certain pollutant concentrations in parts per billion generated by the chemical plants have typically been shown to exhibit the neutrosophic Maxwell model with distribution parameter $\lambda_N = [3, 5]$. Find the probability that the concentrations surpass 8 parts per billion?

Solution: . Let the random variable W denotes the concentrations in parts per billion; then, the required probability can be obtained as

$$P(w > 8) = 1 - P(w \leq 8) \\ = 1 - \eta_N(8) \\ = [0.068, 0.464]. \quad (26)$$

3. Neutrosophic Estimation Procedure

In this section, we discuss the analytical procedure for estimating the parameter of NMD using the most common method of maximum likelihood (ML). A new procedure using neutrosophic statistics for estimating the parameter of NMD is introduced. Let $w_{1N}, w_{2N}, w_{3N}, \dots, w_{mN}$ be the observed interval values sample from NMD with density function $\phi_N(w)$. Assuming the parameter λ_N is unknown in the defined distribution, then $\prod_{i=1}^m \phi_N(w_{iN}, \lambda_N)$ be the joint probability of the observed sample.

Taking the logarithm of the product $\prod_{i=1}^m \phi_N(w_i, \lambda_N)$ provides log-likelihood as

$$\xi_N(w_{iN}, \lambda_N) = \frac{n}{2} \log\left(\frac{2}{\pi}\right) - 3n \log \lambda_N \\ + \log \prod_{i=1}^n w_{iN}^2 - \frac{\sum_{i=1}^n w_{iN}^2}{2\lambda_N^2}. \quad (27)$$

The ML estimate of the unknown λ_N is the value that maximizes $\xi_N(w, \lambda_N)$, i.e.,

$$\hat{\lambda}_N = \max(\xi_N(w_{iN}, \lambda_N)). \quad (28)$$

The ML estimates, namely, $\hat{\lambda}_N$ can be obtained by using the neutrosophic calculus as

$$\frac{\delta \xi_N(w, \vartheta_N)}{\delta \lambda_N} = \left[\frac{\delta \xi_l(w_{il}, \lambda_l)}{\delta \lambda_u}, \frac{\delta \xi_u(w_{iu}, \lambda_u)}{\delta \lambda_l} \right], \quad (29)$$

where $\xi_l(w, \lambda_l) = (n/2) \log(2/\pi) - 3n \log \lambda_l + \log \prod_{i=1}^n w_{il}^2 - (\sum_{i=1}^n w_{il}^2 / 2\lambda_l^2)$ and

$$\xi_u(w, \lambda_u) = \frac{n}{2} \log\left(\frac{2}{\pi}\right) - 3n \log \vartheta_u + \log \prod_{i=1}^n w_{iu}^2 - \frac{\sum_{i=1}^n w_{iu}^2}{2\lambda_u^2}. \quad (30)$$

Simplification of equation (29) provides

$$\frac{\delta \xi_N(w, \lambda_N)}{\delta \lambda_N} = \left[\frac{-3n}{\lambda_l} + \frac{\sum_{i=1}^n w_{il}^2}{\lambda_l^3}, \frac{-3n}{\lambda_u} + \frac{\sum_{i=1}^n w_{iu}^2}{\lambda_u^3} \right]. \quad (31)$$

Equating equation (31) to $[0, 0]$ yields

$$[\hat{\lambda}_l, \hat{\lambda}_u] = \left[\sqrt{\frac{\sum_{i=1}^n w_{il}^2}{3n}}, \sqrt{\frac{\sum_{i=1}^n w_{iu}^2}{3n}} \right], \quad (32)$$

hence proved.

Following the work of Sultan et al. [29], the effectiveness of the neutrosophic ML estimate is also evaluated for an unknown parameter of NMD. A Monte Carlo simulation is run with varying sample sizes and parameter settings to see how the results vary. There are 10^5 simulation runs performed, each one using a sample size of $m = 5, 25, 50, 100,$ and 150 with true parameter λ_N equal to $[2, 2.5]$. In this simulated experiment, the following two metrics are used as performance indicators for each of our simulated data samples:

$$\text{Mean bias}(MB_N) = \frac{\sum_{j=1}^M (\hat{\lambda}_N - \lambda_N)}{M}, \quad (33)$$

where M is the total number of runs in the simulation experiment.

$$\text{Root mean square bias}(RMSB_N) = \sqrt{\frac{\sum_{j=1}^M (\hat{\lambda}_N - \lambda_N)^2}{M}}. \quad (34)$$

For the sake of simulation, all computations are carried out using R software. The metrics MB_N and $RMSB_N$ have been calculated for the abovementioned sample sizes and are given in Table 1.

We can see from the findings in Table 1 that the biases diminish as the sample size m rises. It can infer from the results that the neutrosophic estimate provides more reliable results when the sample size is increased.

4. Simulation Study

In this section, simulated data of 100000 observations from the NMD have been generated with the inverse transformation approach. Random numbers from a given distribution are created using the inverse transformation technique by solving the following equation for Q_{NP} at predetermined values of distributional parameter:

$$Q_{NP} = F^{-1}(u), \quad (35)$$

TABLE 1: Performance of the ML estimator of NMD for simulated data.

Sample size (m)	MB_N	$RMSB_N$
5	(0.01762, 0.01971)	(0.24273, 0.27431)
25	(0.00227, 0.00246)	(0.10453, 0.11697)
50	(0.00137, 0.00156)	(0.07321, 0.08235)
100	(0.00064, 0.00071)	(0.05198, 0.05812)
150	(0.00032, 0.00047)	(0.03621, 0.03924)

where F^{-1} denotes the inverse of a particular distribution function, $u \sim U[0, 1]$, and Q_{NP} is the quantile point of the distribution.

In the case of NMD, equation (35) can be expressed as

$$\frac{2}{\sqrt{\pi}} \gamma \left[\frac{3}{2}, \frac{w^2}{2\lambda_N^2} \right] = u. \quad (36)$$

By solving equation (35) for w at a particular value of the parameter, say $\lambda_N = [1, 1.5]$ and 100000 random values from the uniform distribution resulted in 100000 different neutrosophic samples from NMD. The closed-form expression for equation (36) does not exist because of the intractable nature of $\eta_N(w)$. The function $\eta_N(w)$ cannot be used explicitly for generating random numbers. Alternatively, the quantile points and other useful statistics can be estimated by using R as a programming language. The basic quantile points and other useful descriptive measures for different values of λ_N estimated over 100000 runs are given in Table 2.

Table 2 provides the useful statistics of NMD estimated over simulated data in interval forms due to the fact that the parameter λ_N is not precisely determined. Notice that values of skewness and kurtosis coefficients are invariant and crisp numbers because of the fact that they are do not involve indeterminate parameter in their expressions. Additionally, results of NMD coincide with the conventional model of the Maxwell distribution if upper and lower limits become the same, as given in the last column of Table 2.

5. Real Application

In this part, we have applied our suggested model to COVID-19 mean incubation time data obtained from the source [30]. Infectious illness incubation periods or the time between infection with a microbe and disease manifestation are directly significant to prevention and control. One of the most significant indicators of disease propagation and quarantine measures is the incubation period, which is the time period between infection and the start of symptoms [31]. Explicit models of the incubation time help us better understand how diseases spread. Infectious illnesses have an incubation time that may vary from a few hours, as is usual in the case of severe food poisoning, too many decades, as is the case with HIV and TB [32]. It is helpful in clinical practice for drawing rough estimates about the origins and sources of infection of specific patients and for establishing treatment methods that allow the incubation period to be prolonged. When dealing with a point source epidemic, being aware of the incubation period model allows for

TABLE 2: Descriptive measures and quantile points of NMD for simulated data.

Statistical measures	$\lambda_N = (1, 1.5)$	$\lambda_N = (2, 3)$	$\lambda_N = (4, 4)$
Mean	(1.593, 2.390)	(3.186, 4.780)	(6.373, 6.373)
Standard deviation	(0.672, 1.009)	(1.345, 2.018)	(2.691, 2.691)
Skewness coefficient	(0.526, 0.526)	(0.526, 0.526)	(0.526, 0.526)
Kurtosis	(3.253, 3.253)	(3.253, 3.253)	(3.253, 3.253)
First quantile	(1.102, 1.654)	(2.205, 3.308)	(4.411, 4.411)
Second quantile	(1.532, 2.298)	(3.064, 4.596)	(6.128, 6.128)
Third quantile	(2.012, 3.018)	(4.024, 6.037)	(8.049, 8.049)

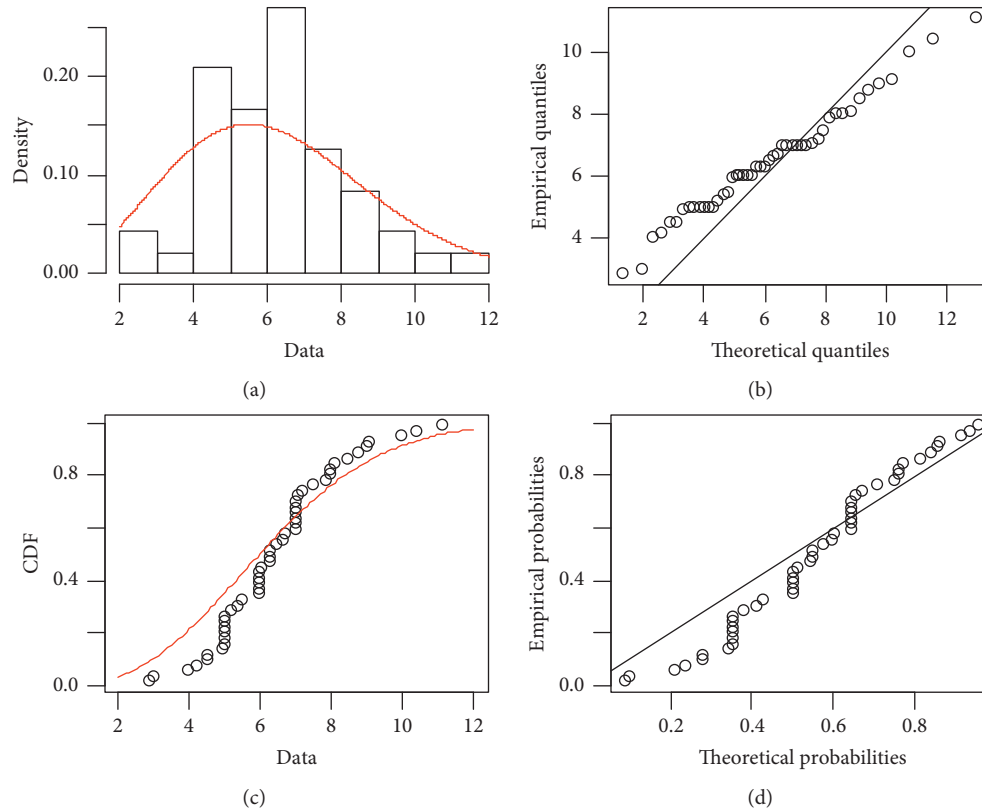


FIGURE 3: Fitting of NMD on incubation period data. (a) Empirical and theoretical dens. (b) Q-Q plot. (c) Empirical and theoretical CDFs. (d) P-P plot.

statistical assessment of exposure time [33]. Furthermore, identifying the incubation time distribution permits statistical assessment of the period of exposure during a point source epidemic, as well as a testing hypothesis to assess whether the pandemic has stopped. The incubation period distribution is important in statistical techniques for reconstructing epidemic curves and forecasting future illness incidence. The incubation period is easily determined from data showing the time of disclosure, such as experimental inoculation data and case travel records, since most infection occurrences are not clearly apparent. A coronavirus that causes severe acute respiratory illness is the cause of COVID-19 [34]. It has expanded to 223 nations and has been labeled a pandemic by the World Health Organization on March 11, 2020, after spreading rapidly. The average incubation time for COVID-19 is 2.87 days; however, the variation is as broad as 17.6 days. Existing studies have

demonstrated that the distribution of the incubation period varies considerably, most likely due to the study population and estimation methods used. The data on incubation periods are not precisely measured. In general, the patient self-reports the beginning date of the symptom, which is deemed accurate but very rare. As a result, determining the incubation period without clear information about the moment of exposure is often challenging. Thus, instead of exact values, the mean incubation period globally from the source is provided with uncertainties instead of crisp numbers, as given in Table 2. Uncertainties in the mean incubation period are created to the strategy designed in [35].

To see Maxwell distribution is one of the reasonable models for describing the incubation period data, an informal graphical approach has been used. The visual fit of the Maxwell distribution on actual mean incubation period data is shown in Figure 3.

TABLE 3: Mean incubation periods with uncertainties for COVID-19.

Mean incubation time			
(7.82, 8.37)	(8.24, 9.88)	(4.95, 5.40)	(7.55, 8.88)
(4.15, 5.89)	(6.87, 7.04)	(5.43, 6.52)	(4.79, 5.89)
(6.87, 7.55)	(5.52, 6.73)	(5.08, 6.93)	(6.62, 7.45)
(3.33, 4.67)	(4.90, 5.57)	(6.61, 7.10)	(3.92, 5.09)
(8.18, 9.24)	(6.62, 7.11)	(5.48, 6.62)	(4.18, 5.97)
(5.50, 7.18)	(9.96, 11.09)	(8.04, 9.44)	(7.37, 8.99)
(5.28, 6.65)	(9.99, 10.70)	(10.66, 11.68)	(8.27, 9.09)
(5.78, 5.12)	(5.43, 6.19)	(4.84, 6.16)	(4.38, 5.40)
(6.45, 7.39)	(6.33, 7.79)	(5.58, 6.02)	(2.21, 3.47)
(7.39, 8.25)	(6.21, 6.86)	(6.01, 7.31)	(6.30, 7.43)
(5.61, 6.64)	(5.82, 6.49)	(5.26, 5.81)	(3.23, 2.21)
(7.51, 8.01)	(4.34, 5.13)	(4.67, 5.23)	(4.31, 4.96)

TABLE 4: Descriptive statistics of mean incubation period data using the proposed neutrosophic approach.

Neutrosophic measures	Fitted results
Mean	(5.81, 6.62)
Variance	(5.92, 7.90)
Kurtosis coefficient	0.12
Skewness coefficient	0.49

The subjective examination of extensively used plots, i.e., frequency distribution, probability plot, quantile plot, and CDF clearly indicates that the Maxwell model is more likely an adequate model for incubation period data. This is inferred from Figure 3 that most real data do not much deviate from the theoretical red lines, suggesting that Maxwell distribution is a reasonable model for the meantime incubation period. More naturally, the incubation period data involving uncertainties (Table 3) cannot be analyzed using the conventional Maxwell distribution. The statistical description of the incubation period data using the density of NMD is given in Table 4.

Table 4 provides the fitted measures of mean incubation period data in the form of intervals for mean and variance due to the estimated uncertainty parameter $\hat{\lambda}_N$. Note that kurtosis and skewness coefficients are crisp values because analytical results as given in equations (13) and (16) do not depend on the estimated parameter value. Thus, the proposed model provides more useful information and efficiently analyzes data involving uncertainties.

6. Conclusions

A novel extension, so-called the neutrosophic Maxwell distribution (NMD) has been presented in this study. This new generalization is designed on the notions of neutrosophic calculus. Various distributional features such as mean, variance, distribution function, and shape coefficients have been explored in the neutrosophic framework. Numerical examples considered in this study demonstrated that theoretical results of NMD are elastic and appropriate to a wide variety of data. The quantile function has been developed to simulate numerical data and investigate the statistical properties of the proposed model. The estimation

approach of maximum likelihood has been established and applied to simulated data. Results from the simulation study indicate that reliable estimates from the proposed model can be obtained with a larger sample size. The COVID-19 incubation time data have been utilized to describe how the proposed model can be implemented in practice. The incubation period for COVID-19 is not precisely measured and hence can easily be analyzed using NMD. It has been shown in the application section that the suggested model can analyze classical datasets and real-world data containing imprecision, vagueness, or uncertainties.

Future studies can be designed to improve the capability of the proposed model for handling indeterminate data in estimation approaches. In addition, this study would be helpful to design improved multivariate models for estimating mean incubation periods for other infectious diseases.

Data Availability

The data used to support the findings of this study are included within the article.

Conflicts of Interest

The authors declare that they have no conflicts of interest.

Acknowledgments

The authors extend their appreciation to the Deanship of Scientific Research at King Khalid University for funding this work under grant number (RGP.2/4/43), received by Mohammed M. Almazah (<https://www.kku.edu.sa>).

References

- [1] J. C. Maxwell, "On the dynamical theory of gases," *Philosophical Transactions of the Royal Society*, vol. 157, pp. 26–78, 1866.
- [2] V. B. Rogankov and L. Z. Boshkov, "Gibbs solution of the van der Waals–Maxwell problem and universality of the liquid–gas coexistence curve," *Physical Chemistry Chemical Physics*, vol. 4, no. 6, pp. 873–878, 2002.
- [3] P. Todorov and D. Bloch, "Testing the limits of the Maxwell distribution of velocities for atoms flying nearly parallel to the walls of a thin cell," *The Journal of Chemical Physics*, vol. 147, no. 19, Article ID 194202, 2017.
- [4] K. Cheng, J. Q. Dong, L. Huang, and L. Yang, "Cover-time distribution of random processes in granular gases," *Physical Review E—Statistical Physics, Plasmas, Fluids, and Related Interdisciplinary Topics*, vol. 98, no. 4, Article ID 042109, 2018.
- [5] F. Rivadulla, "Alternative derivation of the Maxwell distribution of speeds," *Journal of Chemical Education*, vol. 96, no. 9, pp. 2063–2065, 2019.
- [6] F. A. Segovia, Y. M. Gómez, O. Venegas, and H. W. Gómez, "A power Maxwell distribution with heavy tails and applications," *Mathematics*, vol. 8, no. 7, p. 1116, 2020.
- [7] A. Saghir, A. Khadim, and Z. Lin, "The Maxwell length-biased distribution: properties and estimation," *Journal of Statistical Theory and Practice*, vol. 11, no. 1, pp. 26–40, 2017.
- [8] S. Saini, A. Chaturvedi, and R. Garg, "Estimation of stress-strength reliability for generalized Maxwell failure

- distribution under progressive first failure censoring,” *Journal of Statistical Computation and Simulation*, vol. 91, no. 7, pp. 1366–1393, 2021.
- [9] T. N. Sindhu, Z. Hussain, and M. Aslam, “Parameter and reliability estimation of inverted Maxwell mixture model,” *Journal of Statistics & Management Systems*, vol. 22, no. 3, pp. 459–493, 2019.
- [10] S. Chaudhary and S. K. Tomer, “Estimation of stress-strength reliability for Maxwell distribution under progressive type-II censoring scheme,” *International Journal of System Assurance Engineering and Management*, vol. 9, no. 5, pp. 1107–1119, 2018.
- [11] S. Dey and S. S. Maiti, “Bayesian estimation of the parameter of Maxwell distribution under different loss functions,” *Journal of Statistical Theory and Practice*, vol. 4, no. 2, pp. 279–287, 2010.
- [12] A. Chaturvedi and U. Rani, “Classical and Bayesian reliability estimation of the generalized Maxwell failure distribution,” *Journal of Statistical Physics*, vol. 32, no. 1, pp. 113–120, 1998.
- [13] A. Bekker and J. J. J. Roux, “Reliability characteristics of the Maxwell distribution: a Bayes estimation study,” *Communications in Statistics—Theory and Methods*, vol. 34, no. 11, pp. 2169–2178, 2006.
- [14] N. L. Johnson, S. Kotz, and N. Balakrishnan, *Continuous Univariate Distributions*, Vol. 2, John Wiley & Sons, Hoboken, NJ, USA, 1995.
- [15] W. Q. Duan, Z. Khan, M. Gulistan, and A. Khurshid, “Neutrosophic exponential distribution: modeling and applications for complex data analysis,” *Complexity*, vol. 2021, Article ID 5970613, 8 pages, 2021.
- [16] M. Aslam, “Design of sampling plan for exponential distribution under neutrosophic statistical interval method,” *IEEE Access*, vol. 6, pp. 64153–64158, 2018.
- [17] Z. Khan, M. Gulistan, N. Kausar, and C. Park, “Neutrosophic rayleigh model with some basic characteristics and engineering applications,” *IEEE Access*, vol. 9, pp. 71277–71283, 2021.
- [18] M. L. Puri, D. A. Ralescu, and L. Zadeh, “Fuzzy random variables,” *Readings in Fuzzy Sets for Intelligent Systems*, pp. 265–271, 1993.
- [19] Z. Mu, S. Zeng, and P. Wang, “Novel approach to multi-attribute group decision-making based on interval-valued Pythagorean fuzzy power Maclaurin symmetric mean operator,” *Computers & Industrial Engineering*, vol. 155, Article ID 107049, 2021.
- [20] S. Zeng, M. Shoaib, S. Ali, F. Smarandache, H. Rashmanlou, and F. Mofidnakhai, “Certain properties of single-valued neutrosophic graph with application in food and agriculture organization,” *International Journal of Computational Intelligence Systems*, vol. 14, no. 1, pp. 1516–1540, 2021.
- [21] Y. Hu, S. Zeng, L.-A. Carlos, K. Ullah, and Y. Yang, “Social network group decision-making method based on q-rung orthopair fuzzy set and its application in the evaluation of online teaching quality,” *Axioms*, vol. 10, no. 3, p. 168, 2021.
- [22] M. Á. Gil, M. López-Díaz, and D. A. Ralescu, “Overview on the development of fuzzy random variables,” *Fuzzy Sets and Systems*, vol. 157, no. 19, pp. 2546–2557, 2006.
- [23] F. Smarandache, S. Broumi, P. K. Singh et al., “Introduction to neutrosophy and neutrosophic environment,” *Neutrosophic Set in Medical Image Analysis*, pp. 3–29, 2019.
- [24] F. Smarandache, *Neutrosophical Statistics*, Sitech & Education Publishing, Jaffrey, NH, USA, 2014.
- [25] Z. Khan, M. Gulistan, W. Chammam, S. Kadry, and Y. Nam, “A new dispersion control chart for handling the neutrosophic data,” *IEEE Access*, vol. 8, pp. 96006–96015, 2020.
- [26] F. Shah, Z. Khan, M. Aslam, and S. Kadry, “Statistical development of the V_{SQ} -control chart for extreme data with an application to the carbon fiber industry,” *Mathematical Problems in Engineering*, vol. 2021, Article ID 9766986, 11 pages, 2021.
- [27] R. A. K. Sherwani, M. Aslam, M. A. Raza, M. Farooq, M. Abid, and M. Tahir, “Neutrosophic normal probability distribution—a spine of parametric neutrosophic statistical tests: properties and applications,” *Neutrosophic Operational Research*, pp. 153–169, 2021.
- [28] R. A. K. Sherwani, S. Iqbal, S. Abbas, M. Aslam, and A. H. Al-Marshadi, “A new neutrosophic negative binomial distribution: properties and applications,” *Journal of Mathematics*, vol. 2021, Article ID 2788265, 12 pages, 2021.
- [29] S. Sultan, Z. Khan, H. Ayed, A. Brahmia, and A. Amin, “The neutrosophic lognormal model in lifetime data analysis: properties and applications,” *Journal of Function Spaces*, vol. 2021, Article ID 6337759, 9 pages, 2021.
- [30] C. Cheng, D. Zhang, D. Dang et al., “The incubation period of COVID-19: a global meta-analysis of 53 studies and a Chinese observation study of 11 545 patients,” *Infectious Diseases of Poverty*, vol. 10, no. 5, pp. 1–3, 2021.
- [31] C. McAloon, Á. Collins, K. Hunt et al., “Incubation period of COVID-19: a rapid systematic review and meta-analysis of observational research,” *BMJ Open*, vol. 10, no. 8, Article ID e039652, 2020.
- [32] W. Y. T. Tan, L. Y. Wong, Y. S. Leo, and M. P. H. S. Toh, “Does incubation period of COVID-19 vary with age? a study of epidemiologically linked cases in Singapore,” *Epidemiology and Infection*, vol. 148, 2020.
- [33] C. Elias, A. Sekri, P. Leblanc, M. Cucherat, and P. Vanhems, “The incubation period of COVID-19: a meta-analysis,” *International Journal of Infectious Diseases*, vol. 104, pp. 708–710, 2021.
- [34] K. Ejima, K. S. Kim, C. Ludema et al., “Estimation of the incubation period of COVID-19 using viral load data,” *Epidemics*, vol. 35, Article ID 100454, 2021.
- [35] Z. Khan, M. Gulistan, R. Hashim, N. Yaqoob, and W. Chammam, “Design of S-control chart for neutrosophic data: an application to manufacturing industry,” *Journal of Intelligent and Fuzzy Systems*, vol. 38, no. 4, pp. 4743–4751, 2020.